Research Square

Preprints are preliminary reports that have not undergone peer review.
They should not be considered conclusive, used to inform clinical practice,
or referenced by the media as validated information.

In-situ experiments and numerical simulation of ground vibration isolation using concrete row-pile barriers

Ping Xu

plian127@163.com

Zhengzhou University

Fengyi Guo

Zhengzhou University

Ruilin Zhang

Zhengzhou University

Method Article

Keywords: Ground vibration, Concrete row-pile barriers, Vibration isolation, In-situ experiments, Finite element simulation, Wave propagation

Posted Date: November 13th, 2026

DOI: https://doi.org/10.21203/rs.3.rs-11316240/v1

License: This work is licensed under a Creative Commons Attribution 4.0 International License.
Read Full License

Additional Declarations: No competing interests reported.

In-situ experiments and numerical simulation of ground vibration isolation using concrete row-pile barriers

Ping Xu [a,*], Fengyi Guo [a], Ruilin Zhang [a,*]

[a]*School of Water Conservancy and Transportation, Zhengzhou University, Zhengzhou, 450001, P.R. China.*

Abstract: In recent years, ground vibration induced by train operation and other rail-transit activities has become increasingly prominent, creating a growing need for effective vibration isolation measures. This study combines in-situ experiments with finite element simulations to systematically investigate the ground vibration isolation performance of concrete row-pile barriers. Firstly, in-situ experiments were conducted under no-barrier, single-row, and double-row configurations to examine the effects of the number of pile rows and vibration direction on isolation performance. A finite element model was then established and validated against the experimental results. Based on the validated model, parametric analyses were performed to investigate the effects of pile length, pile diameter, pile spacing, number of pile rows, barrier location, and source position. Further dimensionless analysis was conducted by normalizing the pile geometric parameters and source-to-barrier distance with the characteristic Rayleigh wavelength of the site. The results show that the isolation performance of row-pile barriers exhibits pronounced spatial non-uniformity. For single-row barriers, pile length and spacing are the dominant parameters, with effective ranges of approximately 12–16 m and 1–2 m, respectively. For multiple-row barriers, increasing the number of rows improves vibration attenuation but produces diminishing marginal benefits. Local vibration amplification is also observed behind double-row barriers in the near-field oblique region. Finally, the findings provide a scientific basis and engineering reference for the design of concrete row-pile barriers for ground vibration isolation.

Keywords: Ground vibration; Concrete row-pile barriers; Vibration isolation; In-situ experiments; Finite element simulation; Wave propagation.

1. Introduction

In recent years, ground vibration associated with rail transit and other urban activities has become an important environmental concern because vibration can propagate through the ground to

* Corresponding author.
Email address: plian127@163.com (P. Xu); ruilinzhang@zzu.edu.cn (R. Zhang)

nearby buildings, precision laboratories, medical facilities, and other vibration-sensitive facilities. Previous studies have documented the generation and propagation of traffic- and railway-induced ground vibration, emphasizing the importance of source characteristics and transmission paths [1]. When the frequency content of ground vibration approaches the sensitive frequency range of a structure or piece of equipment, significant dynamic responses may occur . Effective control measures are therefore required along the propagation path . Experimental and field studies have further highlighted the influence of wave propagation conditions and barrier-related transmission characteristics on measured ground vibration . These findings provide the basis for investigating practical measures for vibration reduction in the propagation path [2,3]. The practical performance of such measures depends on the barrier configuration and excitation conditions.

Extensive studies have investigated wave barriers for ground-vibration isolation using analytical, numerical, laboratory, and field approaches. Early work established the screening effects of pile rows and clarified the importance of pile–soil interaction, barrier geometry, and impedance contrast [4]. Subsequent studies examined pile rows under moving loads and demonstrated the potential of pile barriers for reducing vibration transmission [5]. Numerical investigations of layered and poroelastic media further showed that soil conditions and wave characteristics can affect the isolation response . Studies of finite and periodic pile configurations have also demonstrated that pile spacing, geometry, and periodicity influence surface-wave attenuation . Analytical and numerical optimization approaches subsequently explored the design of wave barriers and the characteristics of attenuation zones . Field experiments and coupled numerical–experimental studies have provided additional evidence that barrier performance depends on the excitation and site conditions [6]. Other studies have examined train-induced vibration mitigation and the performance of filled or combined barriers, further broadening the range of practical barrier configurations considered . Related studies have also examined dual in-filled trenches and periodic wave barriers for vibration screening and surface-wave isolation.

More recent studies have extended this research toward practical vibration mitigation under transportation and site-specific conditions. Investigations published in recent years have considered topology-optimized barriers and periodic wave-impeding barriers, emphasizing the influence of barrier geometry on vibration reduction . Field-based research has also assessed single and coupled

wave barriers under realistic excitation conditions [7]. Partially embedded periodic piles and novel periodic pile barriers have been investigated to improve surface-wave isolation and broaden the applicable frequency range [8]. Composite barriers and complex band-structure approaches have further clarified the roles of material composition and wave dispersion in vibration isolation . Recent work has also addressed railway-induced vibration in tunnels and buildings, as well as site-specific numerical validation [9]. Exact solutions and multi-row geometric effects have been examined for periodic pile barriers under different wave-propagation conditions .

Recent investigations have also considered the effects of multi-row pile geometry and advanced periodic pile barriers [10]. Other studies have examined composite periodic barriers and wave-dispersion characteristics, including the effects of material composition and band structure [11]. Railway-specific applications and site-oriented numerical studies have further highlighted the influence of soil conditions and propagation environments on vibration isolation [12].

Nevertheless, most existing mechanistic studies focus on idealized wave fields, periodic or simplified barrier assumptions, or a limited set of geometric parameters . Systematic field-validated evidence remains limited regarding how pile length, spacing, diameter, row number, barrier location, and source position jointly affect the spatially non-uniform response of finite concrete row-pile barriers . Several specific knowledge gaps therefore remain. First, although the effects of individual pile parameters have been widely reported, the corresponding threshold behavior and diminishing marginal benefits have rarely been evaluated within a single field-calibrated numerical framework. In particular, the geometric effects of multi-row systems and their dependence on barrier configuration remain incompletely characterized [13]. Second, the additional benefit of multiple pile rows is generally assessed in terms of overall attenuation, whereas its dependence on propagation distance and its spatial concentration in the near field have received less attention [14]. Third, most existing studies consider normal or simplified incident-wave conditions; consequently, directional non-uniformity and possible local amplification associated with oblique incidence of finite multi-row barriers remain insufficiently characterized [15]. These issues motivate a field-validated investigation that links geometric parameters, spatial response, and characteristic wavelength.

To address these gaps, this study combines in-situ experiments with a three-dimensional finite element model to investigate the vibration isolation behavior of finite concrete row-pile barriers

under controlled transient excitation. Field tests were conducted for no-pile, single-row, and double-row configurations using a falling weight deflectometer (FWD), providing measurements of vertical ground vibration at multiple source-to-receiver distances and propagation directions. The FWD is treated here as a controlled transient excitation rather than a direct representation of moving train loading; its dominant frequency is within the frequency range considered relevant to the present site and provides a repeatable basis for comparing barrier configurations. The numerical model was calibrated against the field measurements and subsequently used to quantify the effects of pile length, pile diameter, pile spacing, number of rows, pile arrangement, barrier location, source position, and concrete strength. Specifically, this study aims to: (i) identify threshold effects and diminishing marginal benefits associated with the principal geometric parameters; (ii) clarify the spatial dependence of the additional isolation benefit provided by multiple pile rows; and (iii) characterize directional non-uniformity and local amplification that may arise under oblique incidence. Finally, the numerical results are interpreted using dimensionless geometric parameters normalized by the characteristic Rayleigh wavelength of the site [16]. The resulting field–numerical framework is intended to clarify the scale dependence and spatial characteristics of pile-barrier isolation [17] and to provide site-specific reference ranges for vibration-isolation applications under conditions comparable to those investigated herein [18].

2. In-situ experiments

2.1 Experimental program

To quantitatively evaluate the vibration isolation effect of concrete row piles on ground vibration, this section conducted in-situ tests at the outdoor field test site of the New Campus of Zhengzhou University. The test site is about 40 m × 40 m. It is flat and open, with no other vibration sources nearby. This effectively avoids interference from environmental vibration. The tests were performed under natural site conditions for both excitation and data acquisition. This preserved the natural soil structure, moisture condition, and stress history. As a result, the test results can capture the actual working performance of the row-pile vibration isolation system.

Two pile layout cases were considered: a single-row barrier and a double-row barrier in a front-to-back staggered arrangement, as shown in Figure 1. The pile diameter was 0.4 m, the pile length was 4 m, and the pile spacing (center-to-center distance) was 1.4 m, corresponding to a clear gap of

1.0 m between adjacent piles. For the double-row barrier, the two rows were arranged in a staggered configuration with an inter-row spacing of 1.0 m. A mobile Luoyang shovel was used to drill the holes, and concrete was poured manually to form the piles. Five measurement points were arranged in a straight line along the vibration propagation direction. The first measurement point was 3 m from the vibration source, and the subsequent points were spaced at 2 m intervals, giving source-to-receiver distances of 3, 5, 7, 9, and 11 m (Figure 1).

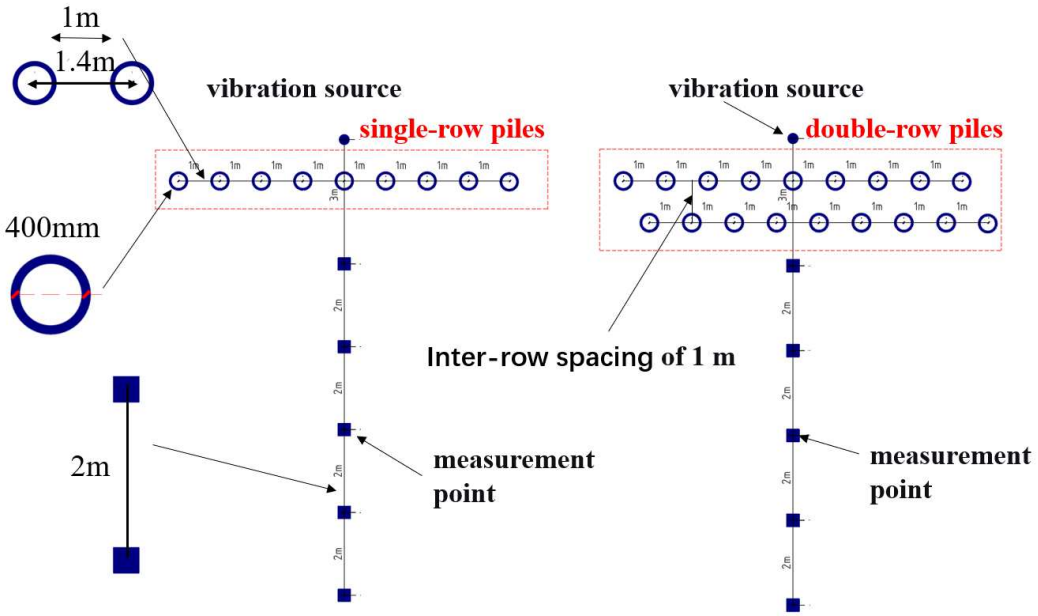


Figure 1. Layout of the field test site and measurement points.

2.1.1 Instrumentation

A falling weight deflectometer (FWD) was used as the excitation source, applying a standard transient impact load at a fixed location. The FWD provides controlled and repeatable excitation, allowing the no-pile, single-row, and double-row configurations to be compared under identical input conditions. The dominant frequency of the FWD impact load was approximately 30 Hz, which partially overlaps with the rail-transit environmental vibration frequency range considered in this study [19]. It should be noted that the FWD represents a localized transient excitation and differs from the loading characteristics of an actual moving train [20]. Therefore, the present test should not be regarded as a direct equivalent of train loading; rather, it was used to investigate the effects of row-pile barriers on the propagation and scattering of ground vibration under controlled conditions. Within the frequency range and site conditions considered in this study, the experimental results provide a reference for understanding the vibration isolation mechanism of row-pile barriers

under rail-transit-induced environmental vibration.

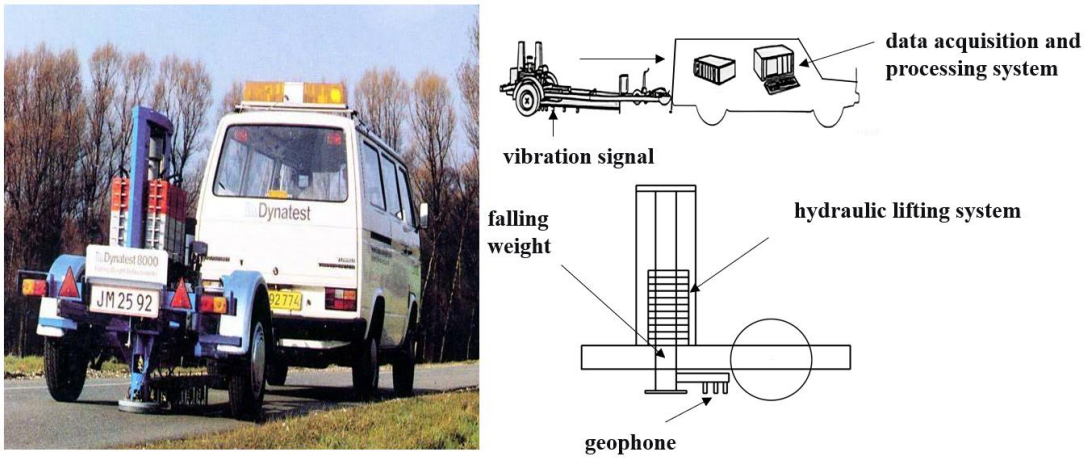


Figure 2. Falling weight deflectometer (FWD) used for field excitation.

2.1.2 Test procedure

The tests followed a controlled comparative design: a no-pile baseline test was performed first, followed by comparative tests with piles. The vibration isolation effect was evaluated by comparing the vibration response data at the same measurement points under each case. The specific test procedure was as follows:

(1) Site preparation: The test site was cleaned and leveled. The ground surface flatness was ensured to meet the requirements for equipment installation and test operations. (Figure 3(a))

(2) Measurement point layout: The first measurement point was placed 3 m from the vibration source. Additional points were then placed every 2 m toward the far field. A total of five measurement points were used. They were located 3, 5, 7, 9, and 11 m from the vibration source, respectively. Sensors were installed at each measurement point.

(3) No-pile baseline test: After the measurement points were arranged, a standard-weight impact load was applied at the vibration source using the FWD. The vibration response data at each measurement point were synchronously acquired and recorded. These data served as the baseline for subsequent evaluation of the vibration isolation effect. (Figure 3(b))

(4) Pile installation: According to the pile positions determined by the test plan, a mobile Luoyang shovel was used to drill the holes. Concrete was then poured manually to form the piles (Figure 3(c)). The single-row barrier and double-row barrier were constructed according to their prescribed layouts.

(5) Post-pile test: After the concrete piles were cured to the required design strength, vibration response tests were conducted again at each measurement point. The loading conditions and measurement point positions were exactly the same as those used in the baseline test (Figure 3(d)).

(6) Data analysis: Test data were collected under each case. The acceleration reduction percentage and amplitude ratio at each measurement point were calculated. The effects of parameters such as the number of pile rows and propagation direction on vibration isolation performance were compared and analyzed.



(a) site preparation and leveling

(b) Measurement Point Layout and No-Pile Baseline Test

(c) Pile Construction

(d) Post-Installation Test

Figure 3. Field test setup and pile installation procedure.

2.1.3 Site conditions

To determine the stratigraphic distribution at the test site and obtain the physical and mechanical parameters of each soil layer, borehole drilling with coring and laboratory tests were carried out at the site. The results show that, from top to bottom, the soil layers at the site are as follows: Layer ① cultivated soil (0.5 m thick), Layer ② silty clay (2.5 m thick), Layer ③ silt (5.0 m thick), and Layer ④ silty clay (10.0 m thick). The stratigraphic identification results are listed in Table 1, and the main physical and mechanical indices of each soil layer are listed in Table 2. The

177 row piles used in the tests were 4 m long, with pile tips embedded in Layer ③ (silt).

178 Table 1. Stratigraphic interpretation of the test site.

Layer	Relative elevation of layer bottom	Thickness (m)	Lithology description
①	0.0～-0.5	0.5	Cultivated soil: yellowish brown, loose, slightly moist, contains a small amount of plant roots and humus.
②	-0.5～-3.0	2.5	Silty clay: yellowish brown, plastic, medium dry strength, medium toughness, no shaking reaction, slightly glossy.
③	-3.0～-8.0	5.0	Silt: yellowish brown, slightly dense, slightly moist, contains a small amount of rust-colored mottling, low dry strength, low toughness, no gloss.
④	-8.0～-18.0	10.0	Silty clay: yellowish brown, plastic, contains a small amount of calcareous concretions, medium dry strength, medium toughness, no shaking reaction, slightly glossy.

179

180 Table 2. Physical and mechanical properties of the soil layers at the test site.

Layer	Soil type	Water content, W_0 (%)	Wet density, ρ (g/cm³)	Compression modulus, E_s (MPa)	Cohesion, c (kPa)	Internal friction angle, φ (°)
②	Silty clay	21.5	1.94	8.9	30.2	22
③	Silt	18.2	1.86	7.1	13.2	27
④	Silty clay	21.7	1.96	9.8	25.2	21.3

181

182 ***2.2 Experimental results***

183 *2.2.1 Effect of pile-row configuration on vibration response*

184 Figure 4 shows the measured peak vertical ground acceleration (PGA) at each measurement

185 point under the three cases: the no-pile case, single-row barrier, and double-row barrier.

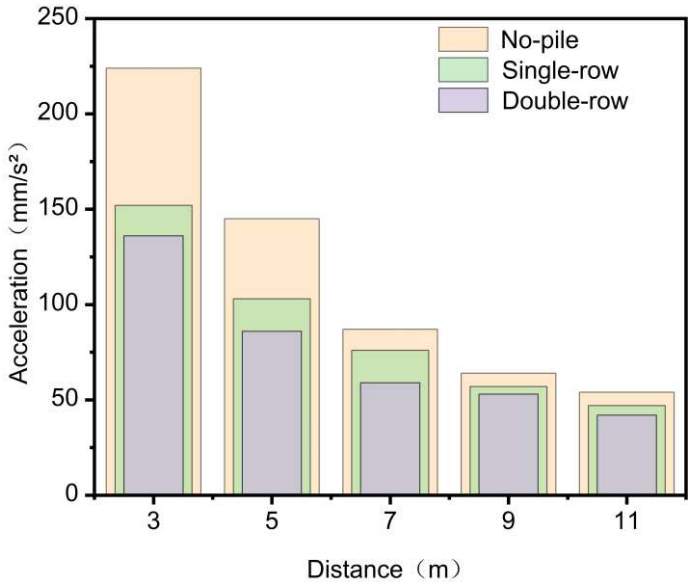


Figure 4. Measured peak vertical ground acceleration (PGA) under different pile-row configurations.

The PGA at each measurement point was highest for the no-pile case, followed by the single-row barrier and then the double-row barrier. This confirms that concrete row-pile barriers can effectively attenuate surface-wave propagation through wave-impedance mismatch and wave scattering [16].

The vibration-isolation benefit of increasing the number of pile rows was most pronounced in the near-field region and gradually converged with increasing propagation distance. At 3 m, the PGA reduction percentages for the single-row and double-row barriers relative to the no-pile case were 32.14% and 39.29%, respectively. The additional gain provided by the double-row barrier was 7.14 percentage points and peaked at approximately 11.7 percentage points at 5 m. This indicates that multiple scattered waves generated by the staggered double-row barrier may have enhanced destructive interference in this region. However, beyond 7 m, the PGA difference between the two pile-barrier configurations narrowed to within 15 mm/s². At 9 m, the difference was only 4 mm/s², indicating that the additional isolation benefit of the double-row barrier had become relatively small. The two attenuation curves therefore gradually approached each other, indicating that the marginal isolation benefit of increasing the number of rows decreases with propagation distance. In the far field, wave field evolution is increasingly governed by diffracted-wave contributions and material damping, making the influence of the pile-row configuration less pronounced [17].

2.2.2 Effect of vibration-wave propagation direction on vibration response

To investigate how the vibration response varies with the wave propagation direction,

measurement points were arranged in two directions for comparative tests. One direction was perpendicular to the pile alignment (90°). The other was oblique at 45° to the pile alignment. The layout is shown in Figure 5. The measured results are shown in Figure 6(a) for the single-row barrier and Figure 6(b) for the double-row barrier.

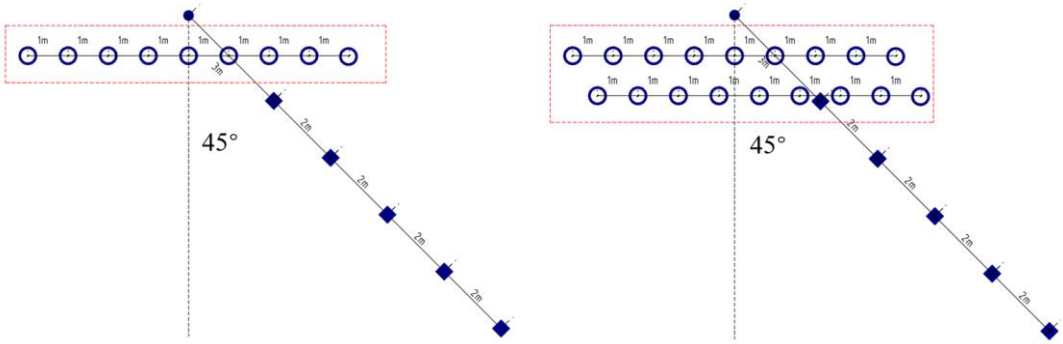


Figure 5. Layout of measurement points for different propagation directions.

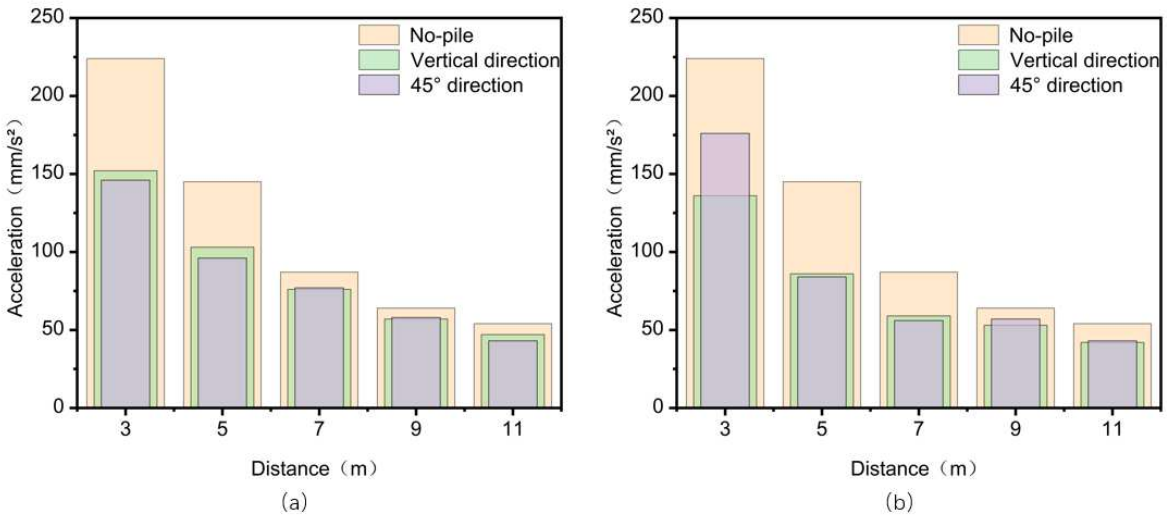


Figure 6. Effect of propagation direction on peak vertical ground acceleration (PGA): (a) single-row barrier; (b) double-row barrier.

For the single-row configuration, the differences in response between the two propagation directions were negligible at all measured distances. At 3 m, the PGA in the 45° direction (146 mm/s²) was only 3.9% lower than that in the perpendicular direction (152 mm/s²), indicating weak directional dependence of the near-field response within the measurement directions and distance range considered in this study [18].

The double-row configuration exhibited a markedly different response, with pronounced

directional dependence in the near field. At 3 m, the PGA in the 45° direction reached 176 mm/s², approximately 29.4% higher than the 136 mm/s² measured in the perpendicular direction, indicating local vibration amplification rather than isolation. This phenomenon may be associated with interference among multiple scattering paths generated by the staggered double-row arrangement. In the field layout, the double-row barrier used a pile spacing of 1.4 m and an inter-row spacing of 1.0 m in a staggered arrangement. These geometric relationships, together with oblique wave propagation, may alter the phase relationships among scattered waves and contribute to local response amplification. However, the present experiments did not directly measure the phase differences between individual scattering paths. Therefore, constructive interference should be regarded as a possible mechanism consistent with the observations rather than as a phase condition directly demonstrated by the experiments. Notably, the same amplification was not observed for the single-row configuration. This difference is consistent with the possible contribution of mutual scattering between the two pile rows, although its specific role requires further verification using frequency-domain and phase information [19].

Consistent with the trend observed in Section 2.2.1, the response differences associated with propagation direction rapidly diminished with increasing distance. At source-to-receiver distances of 5 m and beyond, the relative PGA differences between the two directions were within 5% for both pile configurations, indicating that the far-field radiation pattern became approximately isotropic and was no longer strongly affected by the vibration-wave propagation direction.

Overall,this section investigated the effects of the number of pile rows and propagation direction on ground-vibration response through in-situ experiments. The results show that both single-row and double-row barriers can reduce near-field PGA, while the additional isolation benefit associated with increasing the number of rows gradually converges with propagation distance. Under the experimental conditions considered herein, the response difference between the two pile configurations became markedly smaller beyond approximately 7 m. In addition, local vibration amplification occurred in the 45° oblique near field at 3 m behind the double-row barrier, where the PGA was approximately 29.4% higher than that in the perpendicular direction, whereas no pronounced directional difference was observed for the single-row configuration. These results provide a field basis for quantitative validation of the subsequent numerical model and for the parameter analyses [20].

3. Numerical Simulation

In-situ tests can capture the vibration isolation performance under specific site conditions. However, they cannot systematically examine the coupled effects of multiple parameters. These parameters include pile length, pile diameter, pile spacing, number of pile rows, and layout configuration. To overcome these limitations, this section develops a three-dimensional dynamic numerical model using the ABAQUS finite element platform [21]. All key parameters are obtained from site investigation and test data.

3.1 Development of the Three-Dimensional Numerical Model

Based on a wavelength-based computational-domain criterion, the width and depth of the computational domain should be 1–1.5 times the shear wavelength of interest. At this site, the shear-wave velocity is about 350 m/s, and the dominant test frequency is about 30 Hz. The corresponding Rayleigh wavelength is about 10.8 m, consistent with the wavelength-based attenuation characteristics reported for soil-periodic pile systems [22]. On this basis, the model dimensions were set to 80 m × 80 m × 70 m. The row piles were modeled using the actual field-test design parameters: pile diameter of 0.4 m, pile length of 4 m, and pile spacing (center-to-center distance) of 1.4 m. For the double-row configuration, a staggered arrangement with an inter-row spacing of 1.0 m was adopted to reproduce the field layout. A total of nine piles formed a single-row barrier. The FWD loading plate was simplified as a rigid circular loading surface with a diameter of 0.3 m. It was placed on the ground surface 1 m from the first pile, consistent with the field layout. To avoid non-physical reflections from artificially truncated boundaries, infinite elements were used at the outer boundaries of the model. They were activated by modifying the input-file keywords in ABAQUS. For the mesh size, Kuhlemeyer and Lysmer recommended that the element size should not exceed one-tenth of the wavelength corresponding to the highest frequency of interest. The site Rayleigh wavelength is about 10.8 m; therefore, a 1 m mesh meets this requirement. Trial calculations showed that further refinement changed the PGA at key measurement points by less than 5%. This mesh size was therefore adopted to balance accuracy and efficiency. The model was discretized entirely with hexahedral elements (Figure 7) [23].

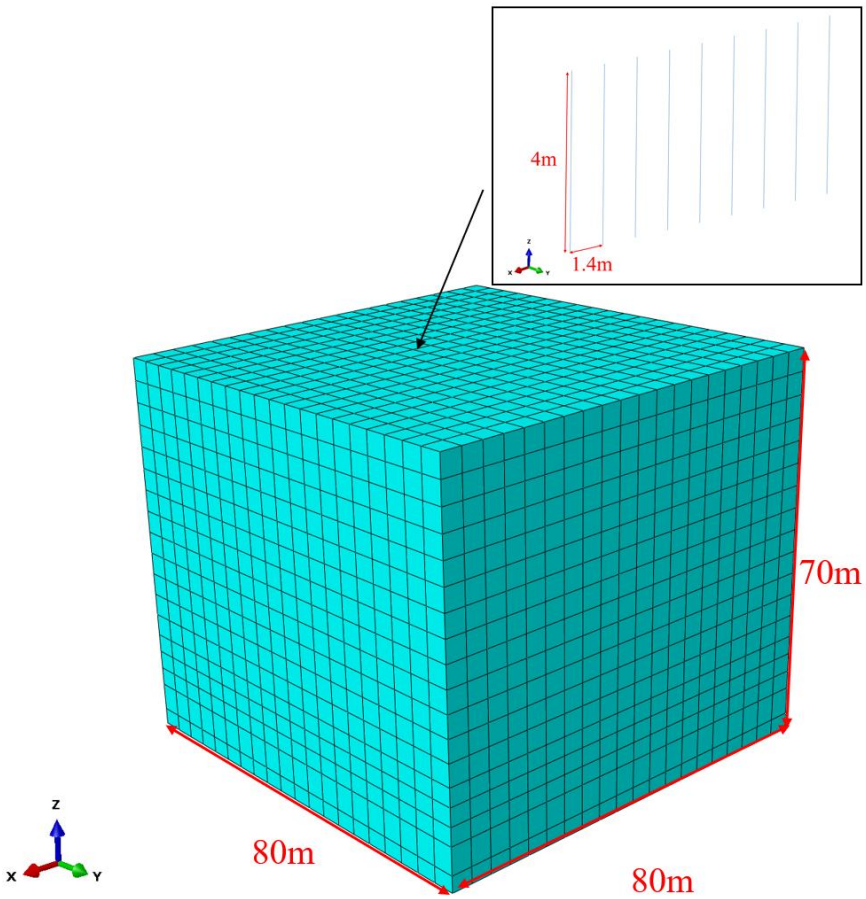


Figure 7. Three-dimensional finite element model.

The soil was modeled using an elastoplastic Mohr-Coulomb constitutive model. The physical and mechanical parameters of each soil layer are listed in Table 3. Under FWD impact loading, the soil strain level was low ($\gamma < 10^{-4}$). Therefore, a small-strain stiffness degradation curve was introduced to modify the elastic modulus. This enabled accurate simulation of the dynamic nonlinear behavior of the soil.

Table 3. Material parameters used in the numerical model.

Layer	Layer thickness (m)	Density (kg/m³)	Elastic modulus (MPa)	Poisson's ratio	Damping ratio
1	3.0	1940	35	0.33	0.03
2	5.0	1860	30	0.33	0.03
3	10.0	1960	55	0.33	0.03
4	52.0	1960	100	0.33	0.03
concrete grade C20		2400	25500	0.16	

Rayleigh damping was used in the dynamic analysis to represent the material damping characteristics of the soil. Based on the measured damping ratio of the site soil, the damping ratio

was taken as ς = 0.03. The mass damping coefficient α and the stiffness damping coefficient β were determined by Equation (1):

$$\begin{cases} \alpha = 2\varsigma\omega_1\omega_2/(\omega_1+\omega_2) \\ \beta = 2\varsigma/(\omega_1+\omega_2) \end{cases} \quad (1)$$

, where ω_1 and ω_2 are the first two natural circular frequencies of the system. The corresponding values of α and β were obtained after estimating the fundamental frequency range from modal analysis. The adopted damping parameters were intended to approximate the energy dissipation characteristics of the soil at the test site, and their adequacy was evaluated by comparing the numerical attenuation response with the measured field response. The validation results indicate that this damping representation adequately captures the wave-attenuation behavior under the site and excitation conditions considered in this study.

The contact condition at the pile–soil interface directly affects the dissipation and transfer of vibration energy between the piles and surrounding soil. A penalty-based frictional contact algorithm was adopted to simulate the interface behavior, with hard contact specified in the normal direction and a tangential friction coefficient of 0.38, calibrated from laboratory direct-shear tests. Unlike a fully bonded assumption, this formulation allows interface separation and sliding, thereby reducing potential distortion in stress transfer around the piles.

3.2 Model Validation and Error Analysis

The attenuation curves of the simulated surface vertical PGA with propagation distance were compared with the field FWD measurements, as shown in Fig. 8 and Table 4. For all three configurations, the numerical simulations reproduced the measured trend of decreasing PGA with increasing propagation distance. The simulated and measured values showed good overall agreement for the no-pile, single-row, and double-row configurations. These results indicate that the numerical model can adequately reproduce the ground-vibration attenuation behavior under the experimental conditions considered and is suitable for subsequent parameter analyses of row-pile barriers [24].

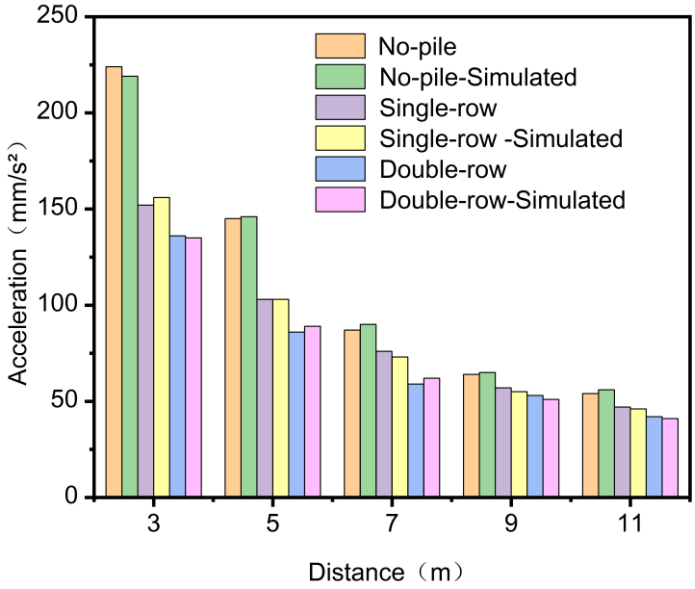


Figure 8. Comparison of measured and simulated peak vertical ground acceleration (PGA) attenuation curves.

Table 4. Comparison of measured and simulated peak vertical ground acceleration (PGA) at different source-to-receiver distances.

Configuration	Data	3 m	5 m	7 m	9 m	11 m
No-pile	Measured	224	145	87	64	54
No-pile	Simulated	219	146	90	65	56
Single-row	Measured	152	103	76	57	47
Single-row	Simulated	156	103	73	55	46
Double-row	Measured	136	86	59	53	42
Double-row	Simulated	135	89	62	51	41

Note: Values are vertical peak ground acceleration (PGA). Overall error metrics are calculated from all 15 measured–simulated data pairs: RMSE = 2.50 mm/s², MAE = 2.13 mm/s², R^2 = 0.9974, mean relative error = 2.62%, and maximum relative error = 5.08%.

4. Numerical Results and Discussion

Based on the model validation, the vibration isolation behavior is discussed in the following order: governing parameters and threshold effects; spatial arrangement and near-field response; synergistic effects and marginal benefits of multiple pile rows; and integrated parameter implications for design. The discussion focuses on identifying controlling factors, threshold effects, and marginal benefits rather than simply listing parameter-dependent variations.

4.1 Numerical Analysis of Single-Row Pile Barriers

For the single-row simulations, the baseline conditions were a pile diameter of 0.4 m, pile

spacing (center-to-center distance) of 1.4 m, pile length of 4 m, C20 concrete, and a barrier center aligned with the vibration source. When a given parameter was investigated, only that parameter was varied while all other baseline conditions were kept unchanged.

Pile length exhibited a clear effective range and diminishing marginal benefit. The improvement in vibration isolation was relatively limited for pile lengths below 8 m, while the reduction ratio increased progressively with increasing pile length. Once the pile length reached approximately 16 m, the incremental benefit associated with further increases in pile length decreased markedly (Fig. 9(a)). This indicates that sufficient embedment depth is important for forming an effective scattering barrier, whereas beyond a certain depth, the additional contribution of pile length to the surface wave field becomes increasingly limited [25].

Pile spacing exhibited a pronounced threshold effect. At small spacings, scattering between adjacent piles maintained relatively strong coupling of the wave field. When the spacing increased beyond 3.0 m, more wave energy could diffract through the gaps between piles, resulting in a marked reduction in vibration isolation; at 4.0 m, the barrier effect became weak (Fig. 9(b)). Thus, pile spacing primarily governs barrier continuity and represents a key geometric parameter for single-row barriers [26].

Pile diameter showed a transition from a pronounced isolation benefit to a gradual saturation effect. For diameters below 0.6 m, increasing the pile diameter enhanced the impedance contrast and scattering between the piles and surrounding soil. Beyond approximately 0.6 m, further increases in pile diameter produced only limited additional isolation benefit (Fig. 9(c)).

Within the parameter range investigated in this study, concrete strength grade had a relatively small influence on the reduction ratio. The variation in reduction ratio from C20 to C60 was limited, indicating that when the piles remain within their normal elastic working range and the geometric conditions are comparable, the isolation response is less sensitive to concrete strength than to pile length, pile spacing, and pile diameter (Fig. 9(d)).

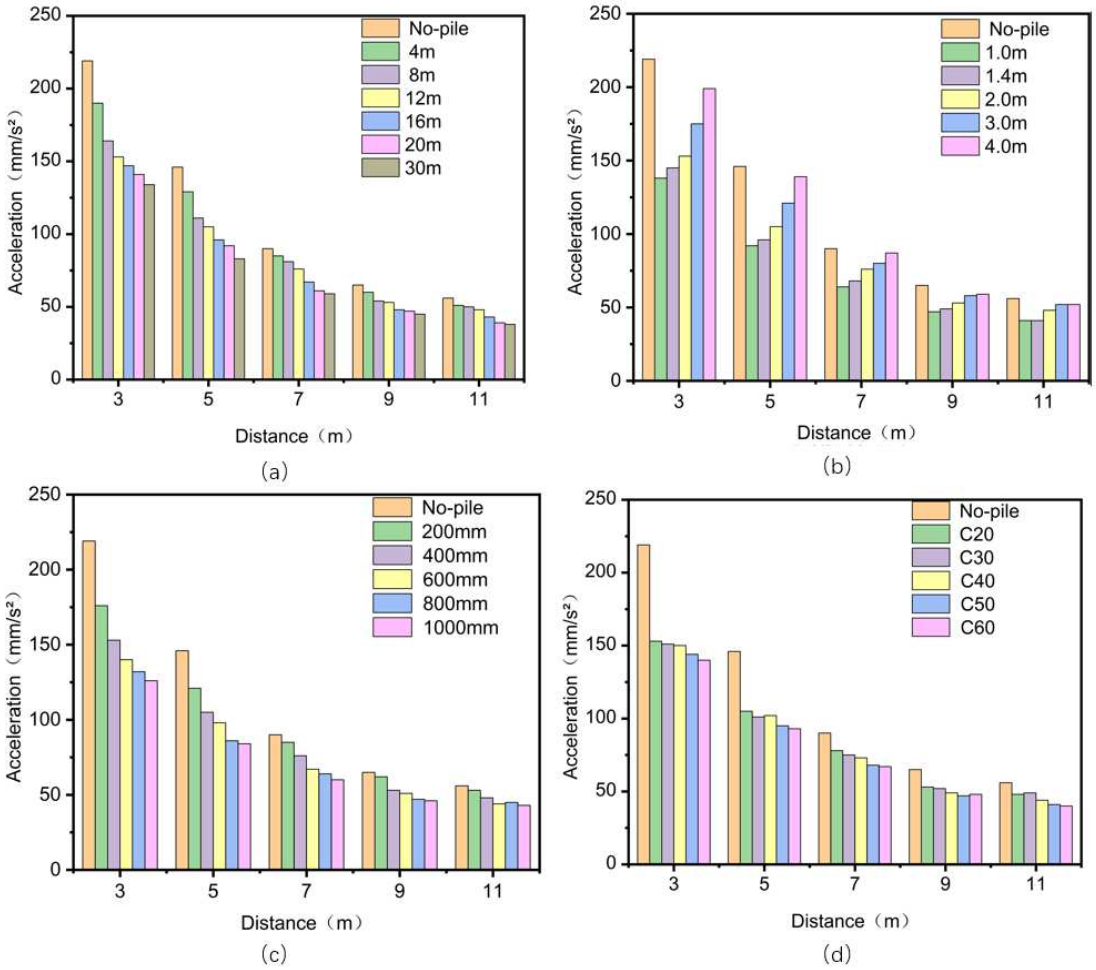


Figure 9. Effects of single-row pile parameters on vibration isolation performance: (a) pile length; (b) pile spacing; (c) pile diameter; (d) concrete strength.

Overall, the vibration isolation performance of the single-row barrier was governed primarily by pile length and pile spacing, followed by pile diameter, whereas the influence of concrete strength was relatively limited within the parameter range considered. Under the conditions investigated in this study, pile lengths of approximately 12–16 m, pile spacings of approximately 1.0–2.0 m, and a pile diameter of approximately 0.6 m were associated with more pronounced improvements in vibration isolation and may serve as reference ranges for the present study. These values should not be interpreted as universal design values; practical applications still require verification against the soil-wave velocity, target frequency, protection distance, and construction conditions of the specific site.

4.2 Spatial Arrangement and Near-Field Response

In addition to geometric parameters such as pile length, pile spacing, and pile diameter, the relative positions of the barrier, vibration source, and protected target can influence near-field wave

propagation and scattering. This section therefore examines the effects of barrier location and the lateral position of the vibration source on the isolation response, with particular emphasis on spatial non-uniformity.

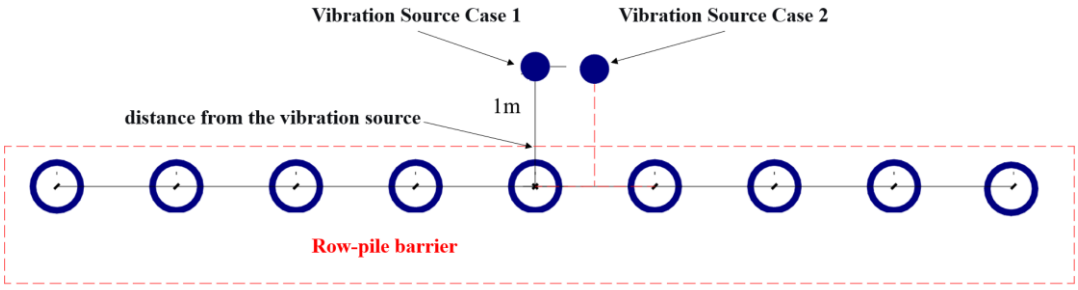


Figure 10. Spatial layout of the vibration source, pile barrier, and measurement points.

The barrier location primarily affected the near-field response in the vicinity of the barrier. [22,23] The numerical results show that when the barrier was located approximately 1.0 m from the vibration source, the reduction ratio on the protected side was approximately 13.3%; when the barrier was moved to approximately 2.5 m from the source, the reduction ratio increased to approximately 20% (Fig. 11(a)). This result indicates that placing the barrier closer to the vibration source does not necessarily lead to greater isolation, because changes in barrier location modify the near-field wave-scattering field and the resulting spatial distribution of the vibration response. When the barrier was located relatively close to the protected target, local vibration enhancement could occur behind the barrier, indicating that the interaction between the barrier, diffracted waves, and the protected-side response should be considered in the spatial arrangement. These observations are specific to the site conditions and parameter ranges investigated in this study.

To further examine the influence of the lateral position of the vibration source, two representative source locations were considered, as illustrated in Fig. 10. In Case 1, the vibration source was aligned with the centerline of a pile, whereas in Case 2, the source was located on the centerline between two adjacent piles.

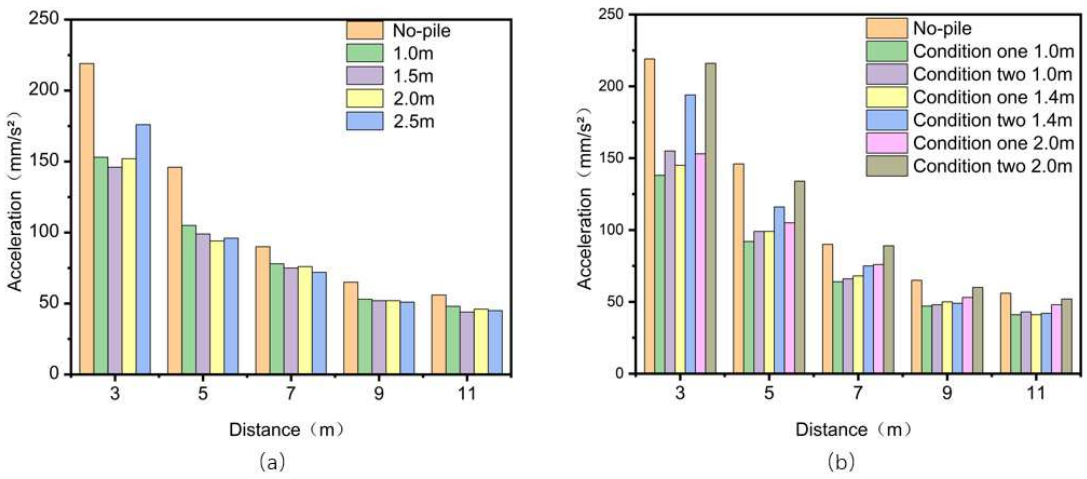


Figure 11. Effects of spatial layout parameters on vibration isolation performance: (a) barrier location; (b) lateral position of the vibration source.

The results indicate that the sensitivity to the lateral source position depended on the center-to-center pile spacing (Fig. 11(b)). [24,25] When the pile spacing was 2.0 m, the difference in the reduction ratio between the two source positions was the most pronounced. As the pile spacing decreased to 1.4 m, the sensitivity to the source position was reduced, although a noticeable difference remained. When the pile spacing was further reduced to 1.0 m, the isolation responses corresponding to the two source positions became relatively close. These 1.4 m and 1.0 m cases are numerical parametric conditions; the field-test center-to-center spacing was 1.4 m, with a 1.0 m clear gap between adjacent 0.4 m-diameter piles. The trend suggests that smaller pile spacing improves the spatial continuity of the barrier and reduces the sensitivity of the isolation response to lateral variations in the vibration-source position.

Overall, the spatial arrangement of the barrier and vibration source mainly affected the near-field response, whereas the influence became less pronounced with increasing propagation distance. The barrier location modifies the local scattering and diffraction field, while pile spacing affects the sensitivity of the isolation response to the lateral position of the vibration source. Therefore, under the conditions investigated in this study, spatial layout should be considered as a secondary design variable after the principal geometric parameters have been determined, rather than represented by a fixed universal spatial relationship. These findings also provide a basis for the subsequent analysis of the synergistic effects and marginal benefits of multiple pile rows.

4.3 Synergistic Effects and Marginal Benefits of Multiple Pile Rows

The multiple-row simulations used a pile diameter of 0.4 m, pile length of 4 m, pile spacing (center-to-center distance) of 1.4 m, inter-row spacing of 1.0 m, a staggered arrangement, and C20 concrete as the baseline condition. Except for the parameter under investigation, all other conditions were kept unchanged. The analysis focused on the effects of the number of rows, pile length, pile spacing, and pile diameter on the vibration-isolation performance and marginal benefits of multiple-row barriers.

Increasing the number of pile rows adds scattering and energy-dissipation paths, thereby further improving near-field vibration isolation [22]. When the number of rows increased from one to three, the reduction ratio increased from approximately 30% to nearly 50%, while the marginal benefit of each additional row gradually decreased (Fig. 12(a)). This indicates that the isolation benefit of multiple pile rows does not increase linearly with row number. Their principal advantage lies in near-field wave field control, whereas the additional benefit generated by continuously adding barriers becomes increasingly limited [27].

The effect of pile length in multiple-row barriers was generally consistent with that observed for the single-row barrier, although the effective pile-length range occurred at a shorter length. Increasing the pile length from 8 to 12 m resulted in a marked increase in the reduction ratio, whereas the increase became more gradual beyond 12 m. When the pile length reached 30 m, the reduction ratio was approximately 70% (Fig. 12(b)). The superposition of scattering between rows enables the multiple-row system to achieve relatively high vibration isolation with shorter piles. Under the conditions investigated in this study, 8–12 m may serve as one reference range for pile length in multiple-row barriers; however, this range still requires verification against site stratigraphy, target frequency, and protection distance [28].

The multiple-row system also exhibited a pronounced threshold effect associated with pile spacing. The isolation performance improved continuously as the center-to-center pile spacing decreased from 4 m to 1 m. When the spacing exceeded 2 m, the isolation effect became markedly limited; at a center-to-center spacing of 1.0 m and below, the simulated reduction ratio reached approximately 75% (Fig. 12(c)). Closely spaced piles enhance wave field coupling between adjacent piles and form a more continuous propagation-path barrier. It should be emphasized that these results reflect the response under the site, excitation conditions, and parameter ranges investigated in this

study and should not be directly interpreted as universal engineering criteria [29].

Compared with the single-row barrier, the multiple-row system was less sensitive to the diameter of an individual pile. A pile diameter of 0.2 m already produced a measurable isolation effect, while increasing the diameter to 0.4 m resulted in a reduction ratio of approximately 50% (Fig. 12(d)). This suggests that, in a multiple-row system, part of the limitation associated with a smaller individual pile diameter may be compensated for by adding pile rows. However, the specific trade-off remains dependent on soil conditions, excitation frequency, and geometric scale..

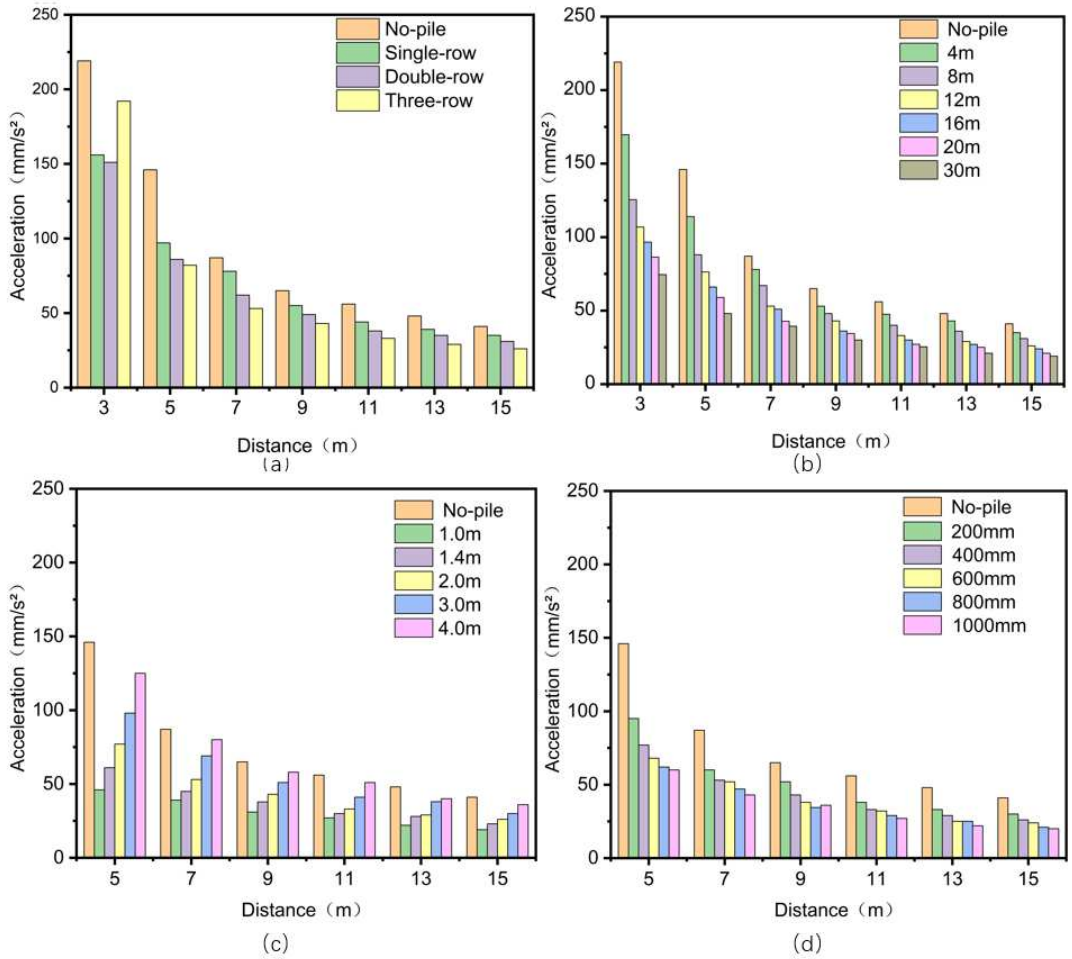


Figure 12. Effects of multiple-row pile parameters on vibration isolation performance: (a) number of rows; (b) pile length; (c) pile spacing; (d) pile diameter.

The difference in vibration isolation performance between staggered and aligned arrangements was relatively limited, with the staggered arrangement providing only a slight improvement that was not pronounced (Figs. 13 and 14). Therefore, under the conditions investigated in this study, the number of rows and pile spacing had more pronounced effects on the isolation performance of the multiple-row system, whereas the specific arrangement can be selected according to site conditions

and construction requirements [30].

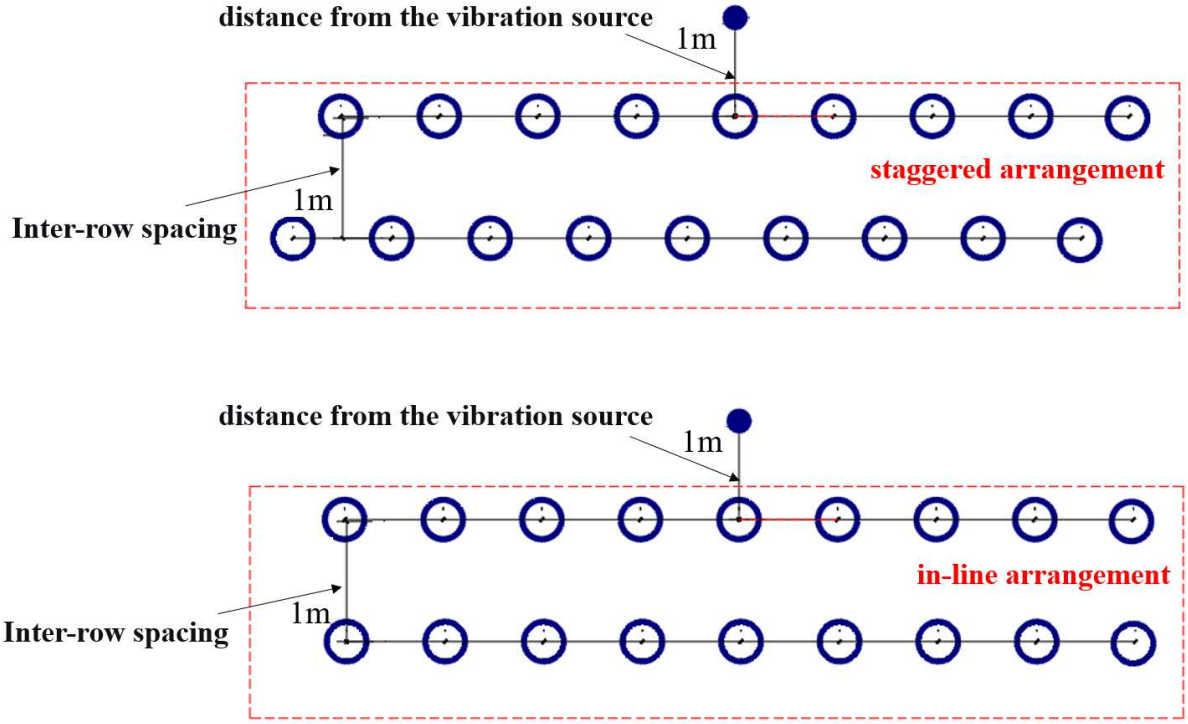


Figure 13. Schematic of staggered and aligned multiple-row pile arrangements.

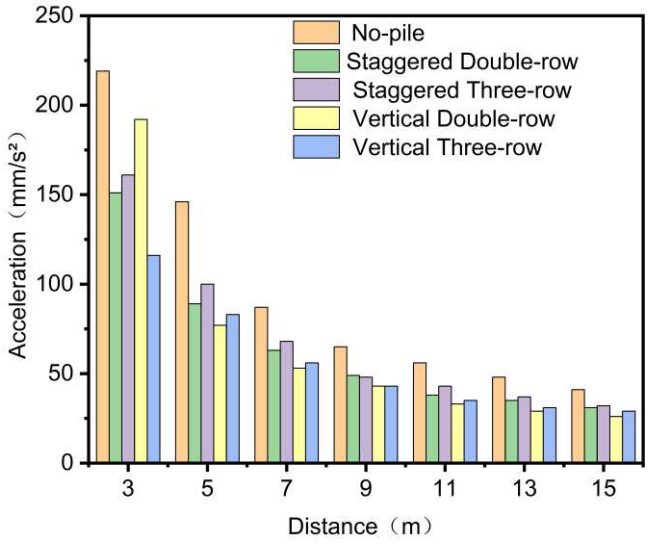


Figure 14. Effect of pile arrangement on vibration isolation performance.

Under the conditions considered in this study, the multiple-row barrier was relatively insensitive to changes in the lateral position of the vibration source. The isolation performance was essentially the same when the source was aligned with the pile center or located on the centerline between two piles (Fig. 15), indicating that multiple scattering in the multiple-row system can, to some extent, reduce the dependence of the isolation response on the incident geometry.

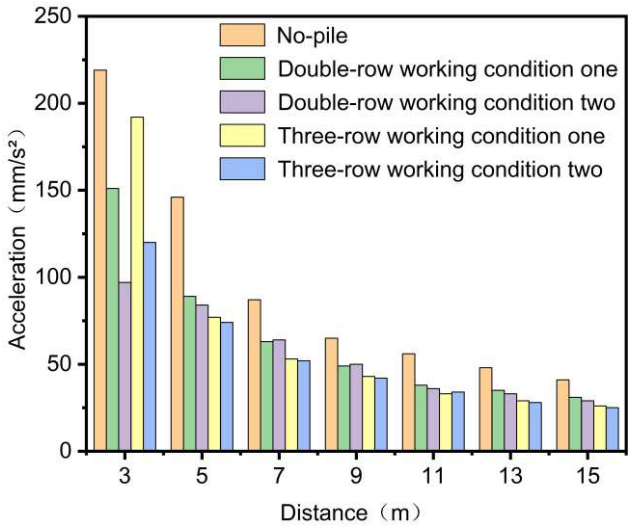


Figure 15. Effect of lateral vibration-source position on vibration isolation performance.

Within the investigated range of 0.5–1.5 m, variations in inter-row spacing produced no pronounced change in the reduction ratio. Therefore, within the parameter range considered in this study, inter-row spacing was not a primary controlling factor. This conclusion should not be extrapolated to larger spacings or different frequency and soil conditions [31].

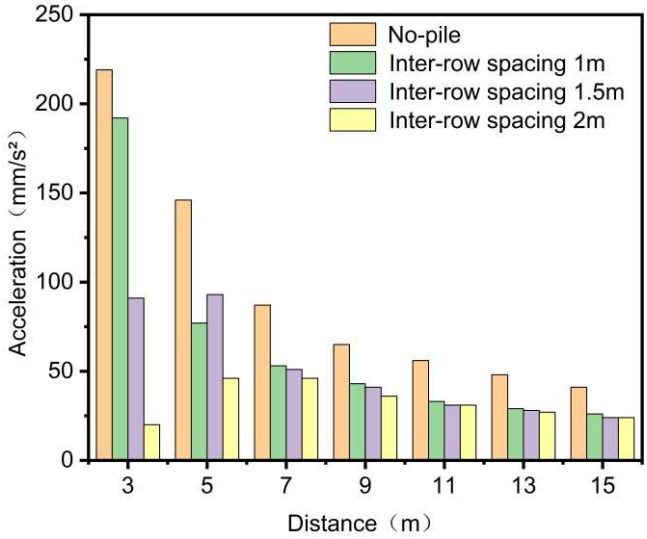


Figure 16. Effect of inter-row spacing on vibration isolation performance.

Overall, under the conditions investigated in this study, two to three pile rows, pile lengths of approximately 8–12 m, and relatively small pile spacing exhibited more pronounced synergistic vibration isolation effects and may serve as reference ranges for the present study. These parameter ranges apply only to the site, excitation frequency, and model parameters considered herein and should not be interpreted as universal engineering recommendations. The principal advantage of the multiple-row system lies in the synergistic isolation achieved through the number of rows and

geometric arrangement rather than simply through increasing the strength of the pile material [32,33].

4.4 Dimensionless Analysis Based on the Characteristic Wavelength

"L/λ""s/λ""d/λ""r/λ""λ" To further elucidate the relationship between the geometric dimensions of the pile barrier and the wave characteristics of the site, a characteristic wavelength was introduced to nondimensionalize the geometric parameters based on the numerical results presented above. The pile length, pile spacing, pile diameter, and source-to-receiver distance were normalized as "L/λ""s/λ""d/λ"and"r/λ", respectively, where"λ"denotes the Rayleigh wavelength corresponding to the dominant excitation frequency of approximately 30 Hz at the test site, which was approximately 10.8 m. This analysis does not introduce additional numerical results; rather, it provides a unified scale-based interpretation of the threshold effects and spatial response characteristics identified in the preceding parameter analyses [15,34].

"L/λ"The normalized pile length provides further insight into the effective scale of the pile barrier relative to the characteristic wavelength. As the pile length increased from 8 to approximately 16 m, L/λ increased from approximately 0.74 to 1.48. In conjunction with the pile-length analysis presented above, the isolation benefit was found to increase progressively with pile length but to exhibit a reduced marginal gain once the pile length reached approximately 16 m. In other words, under the conditions investigated in this study, the marginal isolation benefit tends to decrease when the pile length approaches the order of the characteristic wavelength. This finding suggests that the effective depth of the pile barrier is governed not only by its geometric dimensions but also by the characteristic wave scale of the site.

A similar scale-dependent behavior was observed for pile spacing. For pile spacings of 1–2 m, "s/λ" ranged from approximately 0.09 to 0.19, whereas increasing the spacing to 3–4 m resulted in "s/λ" values of approximately 0.28–0.37, accompanied by a pronounced reduction in isolation performance. Under the conditions investigated herein, when the normalized pile spacing approached approximately"s/λ" = 0.3, diffraction through the gaps between adjacent piles became increasingly important, thereby weakening the continuity of the barrier. Thus, the relative scale of pile spacing with respect to the characteristic wavelength may provide a more meaningful interpretation of the observed threshold effect than the absolute pile spacing alone.

In contrast, the influence of pile diameter was relatively limited when expressed in terms of the characteristic wavelength. Taking the response transition observed at a pile diameter of

approximately 0.6 m as a reference, the corresponding normalized diameter was "d/λ" ≈ 0.056. Further increases in pile diameter resulted in progressively smaller improvements in vibration isolation. This trend is consistent with the preceding pile-diameter analysis and indicates that, within the parameter range investigated in this study, the normalized pile length and pile spacing have a more pronounced relationship with the observed isolation response than the normalized pile diameter.

For the propagation distance, the field measurement points located 3–11 m from the vibration source corresponded to "r/λ" values of approximately 0.28–1.02. As indicated by the field measurements and numerical simulations, the differences in vibration response among the different pile configurations were mainly concentrated in the near-field region and gradually diminished with increasing propagation distance. After normalization by the characteristic wavelength, the same trend remained evident: differences associated with the number of pile rows were more pronounced at relatively small "r/λ", whereas the isolation responses of the different pile configurations gradually converged as "r/λ" increased. This observation indicates that the additional isolation benefit associated with increasing the number of pile rows is strongly dependent on the propagation distance and is related, to some extent, to the characteristic wavelength of the site [35].

"L/λ""s/λ" Overall, the dimensionless analysis indicates that the vibration isolation performance of concrete row-pile barriers is governed not only by the absolute geometric dimensions of the piles, but also by their relative scales with respect to the characteristic wavelength of the site. In particular, the normalized pile length and pile spacing show a clear correspondence with the threshold effects identified in the preceding analyses, while normalization of the propagation distance helps explain why the additional isolation benefit of multiple pile rows is primarily concentrated in the near-field region. It should be emphasized that the characteristic scales and corresponding relationships identified herein are based on the test site, the dominant excitation frequency of approximately 30 Hz, and the parameter ranges considered in this study. They are therefore intended primarily to interpret and generalize the present results and should not be regarded as universal critical values applicable to different sites, excitation frequencies, or geometric scales [36,37].

4.5 Integrated Parameter Assessment and Design Implications

Taken together, the single-row and multiple-row analyses indicate that vibration isolation design using row-pile barriers should prioritize the determination of effective pile length and pile

spacing, followed by the selection of the number of rows and subsequent verification of the spatial arrangement. Pile length governs the effective depth of the barrier, pile spacing controls barrier continuity, and the number of rows determines the degree of multiple-scattering superposition, whereas pile diameter and concrete strength are primarily associated with structural and construction requirements. For engineering applications in which the protected target is located in the near field, the source location, propagation direction, and relative distance between the barrier and protected target should also be checked to avoid local wave field amplification. Because the parameter analyses in this study are based on a single site and a dominant excitation frequency of approximately 30 Hz, site-specific verification should be performed using the dynamic soil parameters and target vibration frequency range of the actual project.

5. Conclusions

This study investigated the ground vibration isolation performance of concrete row-pile barriers and their principal controlling factors through a combination of in-situ experiments and finite element simulations. The numerical model was validated against the field measurements in terms of vibration response under different pile-row configurations and propagation directions, and was subsequently used to systematically examine the effects of pile geometry and spatial arrangement. The main conclusions are as follows:

(1) Concrete row-pile barriers effectively attenuated ground vibration, and their isolation performance exhibited pronounced spatial non-uniformity. Both single-row and double-row barriers provided effective attenuation, while the additional benefit of multiple rows was concentrated mainly in the near-field region and gradually decreased with propagation distance.

(2) Increasing the number of pile rows further improved vibration attenuation, but the marginal isolation benefit decreased with propagation distance and row number. Under the conditions investigated in this study, the additional benefit of the double-row barrier over the single-row barrier was most evident in the near field, whereas the vibration responses of the two configurations gradually converged with increasing propagation distance.

(3) Propagation direction had an important influence on the near-field response of the finite multi-row barrier. At a source-to-receiver distance of 3 m, the PGA behind the double-row barrier in the 45° direction was approximately 29.4% higher than that in the perpendicular direction,

whereas the corresponding difference for the single-row barrier was approximately 3.9%. The directional difference became markedly smaller with increasing propagation distance, demonstrating the directional non-uniformity of the finite barrier response.

(4) Pile length, pile spacing, and the number of rows were the principal parameters governing isolation performance and exhibited clear threshold effects and diminishing marginal benefits. For the single-row barrier, under the conditions investigated herein, pile lengths of approximately 12–16 m and pile spacings of approximately 1–2 m were associated with more pronounced improvements in vibration isolation. The influence of pile diameter gradually approached saturation beyond approximately 0.6 m, whereas concrete strength had a relatively limited influence within the investigated range. For multiple-row barriers, increasing the number of rows and reducing pile spacing further improved vibration attenuation, but the additional benefit gradually diminished.

(5) The scale-based analysis showed that the observed parameter thresholds can be interpreted in relation to the characteristic Rayleigh wavelength of the site. Under the conditions investigated in this study, the normalized pile length, pile spacing, and propagation distance provided a consistent scale-based description of the parameter sensitivity and near-field concentration of the additional benefit of multiple rows. These relationships are intended to interpret the present results and should not be regarded as universal critical values for different sites, excitation frequencies, or geometric scales.

The in-situ experiments employed transient FWD impact loading, which differs from the loading characteristics of actual moving trains, and the parameter analyses were based on a single site with a dominant excitation frequency of approximately 30 Hz. Future studies should therefore incorporate realistic train loads, different geological conditions, and a broader range of excitation frequencies, together with frequency-domain and wave-field analyses, to further verify the applicability and mechanisms of finite multi-row pile barriers.

Declarations

Availability of data and material

The datasets generated and/or analyzed during the current study are available from the corresponding authors upon reasonable request.

615 ***Competing interests***

616 On behalf of all authors, the corresponding author states that there is no conflict of interest.

617 ***Funding***

618 This work was supported by the Zhengzhou University Fund.

619 ***Authors' contributions***

620 Ping Xu contributed to the conceptualization and supervision of the study. Fengyi Guo conducted
621 the field experiments and numerical simulations, performed the data analysis, and prepared the
622 manuscript. Ruilin Zhang contributed to the data analysis, conceptualization, and supervision of the
623 study, and assisted with the revision of the manuscript. All authors read and approved the final
624 manuscript.

625 ***Acknowledgements***

626 This research was financially supported by the China Postdoctoral Science Foundation under Grant
627 Number GZC20261781, for which the authors are grateful.

628 **References**

629 [1]. Kaynia AM, Madshus C, Zackrisson P. Ground vibration from high-speed trains: prediction an
630 d countermeasure. J Geotech Geoenviron Eng. 2000;126(6):531–537. doi:10.1061/(ASCE)109
631 0-0241(2000)126:6(531)
632 [2]. Lombaert G, Degrande G, Clouteau D. Numerical modelling of free field traffic-induced vibra
633 tions. Soil Dyn Earthq Eng. 2000;19(7):473–488. doi:10.1016/S0267-7261(00)00024-5
634 [3]. Lombaert G, Degrande G. Experimental validation of a numerical prediction model for free fie
635 ld traffic induced vibrations by in situ experiments. Soil Dyn Earthq Eng. 2001;21(6):485–497.
636 doi:10.1016/S0267-7261(01)00017-3
637 [4]. Connolly DP, Marecki GP, Kouroussis G, et al. The growth of railway ground vibration proble
638 ms—a review. Sci Total Environ. 2016;568:1276–1282. doi:10.1016/j.scitotenv.2015.09.101
639 [5]. Çelebi E, Kırtel O. Field experiments on wave propagation and vibration isolation by using wa
640 ve barriers. Soil Dyn Earthq Eng. 2009;29(5):824–833. doi:10.1016/j.soildyn.2008.08.007
641 [6]. Dijckmans A, Ekblad A, Smekal A, et al. Efficacy of a sheet pile wall as a wave barrier for rail
642 way induced ground vibration. Soil Dyn Earthq Eng. 2016;84:55–69. doi:10.1016/j.soildyn.20
643 16.02.001
644 [7]. Alzawi A, El Naggar MH. Full scale experimental study on vibration scattering using open an
645 d in-filled (GeoFoam) wave barriers. Soil Dyn Earthq Eng. 2011;31(3):306–317. doi:10.1016/
646 j.soildyn.2010.08.010
647 [8]. Ulgen D, Toygar O. Screening effectiveness of open and in-filled wave barriers: a full-scale ex

perimental study. Constr Build Mater. 2015;86:12–20. doi:10.1016/j.conbuildmat.2015.03.098
[9]. Thompson D, Jiang J, Toward M, et al. Reducing railway-induced ground-borne vibration by using open trenches and soft-filled barriers. Soil Dyn Earthq Eng. 2016;88:45–59. doi:10.1016/j.soildyn.2016.05.009
[10]. Kattis SE, Polyzos D, Beskos DE. Modelling of pile wave barriers by effective trenches and their screening effectiveness. Soil Dyn Earthq Eng. 1999;18(1):1–10. doi:10.1016/S0267-7261(98)00032-3
[11]. Kattis SE, Polyzos D, Beskos DE. Vibration isolation by a row of piles using a 3-D frequency domain BEM. Int J Numer Methods Eng. 1999;46(5):713–728. doi:10.1002/(SICI)1097-0207(19991020)46:5<713::AID-NME693>3.0.CO;2-U
[12]. Cai YQ, Ding G, Xu CJ. Amplitude reduction of elastic waves by a row of piles in poroelastic soil. Comput Geotech. 2009;36(3):463–473. doi:10.1016/j.compgeo.2008.08.015
[13]. Lu JF, Xu B, Wang JH. Numerical analysis of isolation of the vibration due to moving loads using pile rows. J Sound Vib. 2009;319(3–5):940–962. doi:10.1016/j.jsv.2008.06.032
[14]. Lu JF, Xu B, Wang JH. A numerical model for the isolation of moving-load induced vibrations by pile rows embedded in layered porous media. Int J Solids Struct. 2009;46(21):3771–3781. doi:10.1016/j.ijsolstr.2009.06.022
[15]. Pu X, Shi Z. Periodic pile barriers for Rayleigh wave isolation in a poroelastic half-space. Soil Dyn Earthq Eng. 2019;121:75–86. doi:10.1016/j.soildyn.2019.02.029
[16]. Qiu B, Limam A, Djeran-Maigre I. Numerical study of wave barrier and its optimization design. Finite Elem Anal Des. 2014;84:1–13. doi:10.1016/j.finel.2014.02.002
[17]. Liu J, Feng G, Zhang J, et al. Vibration isolation mechanism of concrete piles for Rayleigh waves on sand foundations. Shock Vib. 2018;2018:6285491. doi:10.1155/2018/6285491
[18]. Gao GY, Zhang QW, Chen J, et al. Field experiments and numerical analysis on the ground vibration isolation of wave impeding block under horizontal and rocking coupled excitations. Soil Dyn Earthq Eng. 2018;115:507–512. doi:10.1016/j.soildyn.2018.09.015
[19]. Kouroussis G, Connolly DP, Verlinden O. Railway-induced ground vibrations—a review of vehicle to soil interactions. Soil Dyn Earthq Eng. 2014;57:1–14. doi:10.1016/j.soildyn.2013.10.001
[20]. Kouroussis G, Connolly DP, Olivier B, Laghrouche O, Alves Costa P. Railway cuttings and embankments: experimental and numerical studies of ground vibration. Sci Total Environ. 2016;557–558:110–122. doi:10.1016/j.scitotenv.2016.03.016
[21]. Yarmohammadi F, Rafiee-Dehkharghani R, Behnia C, et al. Design of wave barriers for mitigation of train-induced vibrations using a coupled genetic-algorithm/finite-element methodology. Soil Dyn Earthq Eng. 2019;121:262–275. doi:10.1016/j.soildyn.2019.03.007

[22]. Ma M, Jiang B, Gao J, et al. Experimental study on attenuation zone of soil-periodic piles system. Soil Dyn Earthq Eng. 2019;126:105738. doi:10.1016/j.soildyn.2019.105738

[23]. Kuhlemeyer RL, Lysmer J. Finite element method accuracy for wave propagation problems. J Soil Mech Found Div. 1973;99(5):421–427. doi:10.1061/JSFEAQ.0001885

[24]. Ma XF, Cao MY, Gu XQ, et al. Vibration-isolation performance of a pile barrier in an area of soft soil in Shanghai. Shock Vib. 2020;2020:8813476. doi:10.1155/2020/8813476

[25]. Gao GY, Li ZY, Qiu C, et al. Three-dimensional analysis of rows of piles as passive barriers for ground vibration isolation. Soil Dyn Earthq Eng. 2006;26(11):1015–1027. doi:10.1016/j.soildyn.2006.02.005

[26]. Toygar O, Ulgen D, Fidan NB. Assessing vibration isolation performance of single and coupled wave barriers through field experiments. Constr Build Mater. 2022;354:129156. doi:10.1016/j.conbuildmat.2022.129156

[27]. Ouakka S, Verlinden O, Kouroussis G. Railway ground vibration and mitigation measures: benchmarking of best practices. Railw Eng Sci. 2022;30:1–22. doi:10.1007/s40534-021-00264-9

[28]. Liu YZ, Yu SS, Liu Z, et al. A field experiment on surface wave isolation by partially embedded periodic pile barriers. J Vib Control. 2023;29(3–4):871–881. doi:10.1177/10775463211054254

[29]. Zhao C, Chen C, Zeng C, et al. Novel periodic pile barrier with low-frequency wide bandgap for Rayleigh waves. Int J Mech Sci. 2023;243:108006. doi:10.1016/j.ijmecsci.2022.108006

[30]. Li Z, Ma MQ, Jiang B, et al. Performance of rubber-concrete composite periodic barriers applied in attenuating ground vibrations induced by metro trains. Eng Struct. 2023;285:116027. doi:10.1016/j.engstruct.2023.116027

[31]. Chen X, Wang Y, Meng F, et al. Isolation effect analysis of periodic pile barriers for Rayleigh waves using complex band diagram. Comput Geotech. 2023;158:105370. doi:10.1016/j.compgeo.2023.105370

[32]. Cao S, Li D, Yin J, et al. Effect of periodic vibration-isolation piles on soil vibration in deep-buried tunnels of suburban railways. Sci Prog. 2024;107(4):368504241282801. doi:10.1177/00368504241282801

[33]. Wu M, Wang B, Ba Z, et al. Vibration isolation of infinitely periodic pile barriers for anti-plane shear waves: an exact series solution. Soil Dyn Earthq Eng. 2024;176:108347. doi:10.1016/j.soildyn.2023.108347

[34]. Yu C, Liu J, Feng G, et al. Study on the effect of multi-row pile geometric parameters on the effective isolation zone. Transp Res Rec. 2025;2679(5):661–674. doi:10.1177/03611981241304761

718 [35]. Pu X, Meng Q, Shi Z. Experimental studies on surface-wave isolation by periodic wave ba
719 rriers. Soil Dyn Earthq Eng. 2020;130:106000. doi:10.1016/j.soildyn.2019.106000
720 [36]. Feng D, Paolucci R, Mazzieri I, et al. High-speed railway-induced ground and building vi
721 bration: numerical validation of a spectral element analysis-based sub-model method. Soil Dy
722 n Earthq Eng. 2024;179:108560. doi:10.1016/j.soildyn.2024.108560
723 [37]. Jayawardana P, Thambiratnam DP, Perera N, et al. Dual in-filled trenches for vibration mit
724 igation and their predictions using artificial neural network. Soil Dyn Earthq Eng. 2019;122:10
725 7–115. doi:10.1016/j.soildyn.2019.04.006
726